UNIVERSITY *of York*

This is a repository copy of *Differential cross sections and polarization observables from CLAS K* photoproduction and the search for new N* states*.

White Rose Research Online URL for this paper:
https://eprints.whiterose.ac.uk/id/eprint/136365/

Version: Published Version

White Rose
university consortium
Universities of Leeds, Sheffield & York

eprints@whiterose.ac.uk
https://eprints.whiterose.ac.uk/
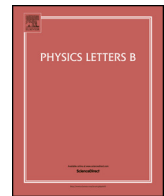
Differential cross sections and polarization observables from CLAS K^* photoproduction and the search for new N^* states

The CLAS Collaboration

ABSTRACT

The reaction $\gamma p \rightarrow K^{*+}\Lambda$ was measured using the CLAS detector for photon energies between the threshold and 3.9 GeV at the Thomas Jefferson National Accelerator Facility. For the first time, spin-density matrix elements have been extracted for this reaction. Differential cross sections, spin density matrix elements, and the Λ recoil polarization are compared with theoretical predictions using the BnGa partial wave analysis. The main result is the evidence for significant contributions from $N(1895)1/2^-$ and $N(2100)1/2^+$ to the reaction. Branching ratios for decays into $K^*\Lambda$ for these resonances and further resonances are reported.

1. Introduction

The thresholds of new channels in photoproduction provide a promising way to search for new baryon resonances or to study their properties. At and just above a threshold, low-spin resonances can often be identified which otherwise may be hidden behind dominating higher-spin resonances. The $N(1535)1/2^-$ resonance with spin $J = 1/2$ and negative parity is the most prominent feature of η photoproduction and hard to find in photoproduction of pions. The $N(1710)1/2^+$ is clearly seen in $\gamma p \rightarrow K^+\Lambda$ while it has been controversially discussed in πN elastic scattering. At or just above the $K^{*+}\Lambda$ threshold at 2007 MeV, a number of missing resonances is expected. In particular, the negative-parity states are predicted to have large couplings to $K^{*+}\Lambda$ [1] and might reveal their existence in photoproduction of this final state. The isospin of the Λ is zero, so any resonance decaying into $K^{*+}\Lambda$ must belong to the nucleon sector. The $K^{*+}\Lambda$ threshold falls into a range where several nucleon resonance are reported but only two of them, $N(1900)3/2^+$ and $N(1875)3/2^-$, are listed in the RPP14 [2] with three-star status. Hence it is interesting to study the reaction $\gamma p \rightarrow K^{*+}\Lambda$ and to search for baryon resonances that may contribute to the reaction.

In this Letter, we report on the first measurement of the spin density matrix elements of $K^{*+}(892)$ mesons observed in the reaction chain:

$$\gamma p \rightarrow K^{*+}(892)\Lambda \, ; \, \Lambda(\mathit{missing})$$

$$K^{*+}(892) \rightarrow K_S\pi^+ \, ; \, K_S \rightarrow \pi^+\pi^- . \qquad (1)$$

For most of the data presented here, the Λ is reconstructed as a missing particle. For the determination of the Λ recoil polarization, the neutral kaon is treated as a missing particle.

2. Data and data analysis

The experiment used the CEBAF Large Acceptance Spectrometer (CLAS) [3] at the Thomas Jefferson National Accelerator Facility. Real photons were produced by bremsstrahlung from a 4.02 GeV electron beam from the Continuous Electron Beam Accelerator Facility (CEBAF) incident on a thin gold foil. The photon energy was determined event-by-event with an energy resolution of about 2–3 MeV by measuring the recoil electron energy in a dipole magnetic field. The tagged photons were collimated and then impinged on a 40 cm long liquid hydrogen target positioned near the center of the CLAS spectrometer. The CLAS detector has a toroidal magnetic field, along with tracking drift chambers and high-precision timing scintillators used to identify particles emanating from the target in coincidence with the tagged photon. Details of the CLAS detector are given in Ref. [3].

Data selection and a method to subtract the background are described in detail in Ref. [4] where results on differential cross sections were fitted with Legendre polynomials. In Ref. [4], the momenta of the three pions from the decay sequence $K^{*+} \rightarrow K_S^0\pi^+ \rightarrow \pi^+\pi^-\pi^+$ were measured, and the Λ was identified via its missing mass. The same data selections (particle identification, vertex cuts, *etc.*) are used here. We outline here the major steps.

K_S candidates are defined by a $M_{K_S} \pm 15$ MeV mass cut while the rare events with both $M(\pi_1^+\pi^-)$ and $M(\pi_2^+\pi^-)$ falling into this window are removed. Integrated over all data, the K_S has a signal to background ratio of 2:3 and a mass resolution of
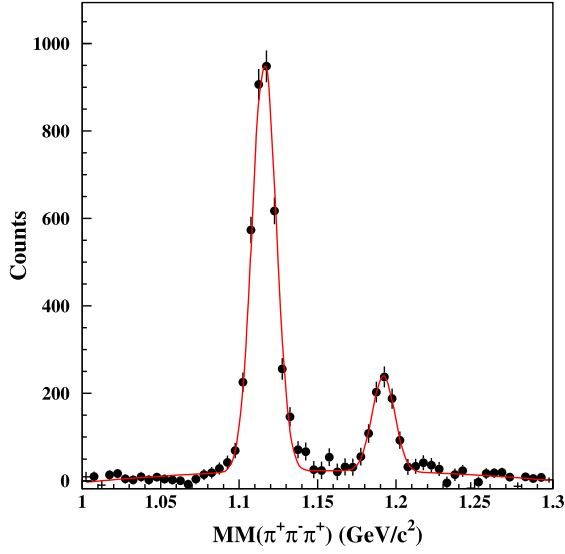
Fig. 1. Example of two Gaussians plus a second order polynomial fit to the reconstructed Λ and Σ^0 missing mass peaks (adapted from Ref. [4]).

Fig. 2. Example of a fit eliminating $\Sigma(1385)$.

$\sigma \simeq 6$ MeV. Events in the K_S side bins (see Fig. 2 in Ref. [4]) are subtracted. In the event-based likelihood method described below, they enter the calculation with negative weight. Further, the missing mass of the three pions, *i.e.*, the mass of the Λ candidate, is required to fall into the window $M_\Lambda \pm 35$ MeV. Fig. 1 shows the distribution of the missing mass recoiling against the $\pi^+\pi^-\pi^+$ system. The signals due to Λ and Σ^0 are seen.

The resulting event sample is still not yet free of background. The main source is due to the reaction $\gamma p \rightarrow K_S \Sigma^{*+}(1385)$ with $\Sigma^{*+}(1385) \rightarrow \Lambda\pi^+$ but also higher mass Σ^*'s resonances contribute to the background. For the present analysis, we used four background-subtraction methods: one consisting of a series of cuts, the other three exploit a variant of the Q-factor method developed in Ref. [5]. The motivation for investigating different background subtraction methods is to estimate the systematic uncertainties associated with the different methods. In a fifth method, we use a Monte Carlo simulation of the background.

In the first method, two additional cuts were applied: the missing mass recoiling against the K_S should not be compatible with the Σ^0 mass, and the three-pion mass should be consistent with the $M(K^{*+}(892))$ mass (*i.e.*, $M(\pi^+\pi^-\pi^+)$ between 850 and 935 MeV).

In the second method we veto the Σ^0 mass as above and apply the Q-factor method to identify the $K^{*+}(892)$ mesons. The $\pi^+\pi^-\pi^+$ mass distribution is fitted for every 100 MeV bin in photon energy and nine bins in $\cos\theta_{K_S}$ as a sum of a Breit–Wigner with the 892 MeV mass and 50 MeV width and a polynomial background. Every event with a given $\pi^+\pi^-\pi^+$ mass has the probability Q to be a $K^{*+}(892)$:

$$Q\left(K^*(892)\right) = \frac{Signal}{Signal + Background} . \tag{2}$$

When all events are weighted with the Q-factor, the K^* signal emerges without background.

In the third method, the Q-factor is first applied to remove events that are compatible with $K^{*+}\Sigma^0$ production. The distribution of missing masses recoiling against the K_S (for fixed energy and $K^{*+}(892)$ angle) is fitted as a sum of a Breit–Wigner function (with $M = 1383$ MeV and $\Gamma = 36$ MeV) and a polynomial background (see Fig. 2) and the Q-factor is calculated. Subsequently, a second Q-factor is determined to extract the $K^{*+}(892)$ in the presence of a $\pi^+\pi^-\pi^+$ background.
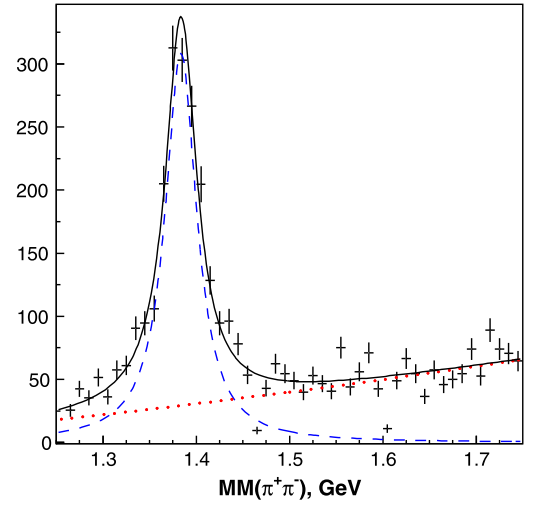
The fourth method is a variant of method 2 but the Breit–Wigner function is replaced by a convolution of Breit–Wigner function with the $M = 892$ MeV and $\Gamma = 50$ MeV and a Gaussian, the so-called Voigt function. The Gaussian resolution is determined in the fit to $0 < \sigma < 5$ MeV. Fig. 3 shows a few examples of fits using a Voigt function. Although the fits shown in the figure are not ideal, the consistency between the fit results and the other methods to obtain the signal give us confidence that the uncertainties are handled properly.

In the fifth method, events due to $\gamma p \rightarrow K_S \Sigma^+(1385)$, $\Sigma^+(1385) \rightarrow \Lambda\pi^+$, and due to $\gamma p \rightarrow K_S \Sigma^+(1800)$, $\Sigma^+(1800) \rightarrow \Lambda\pi^+$, are generated with phase space distributions, and reconstructed with the CLAS event reconstruction program. $\Sigma(1800)$ is supposed to represent the contribution of higher mass Σ^* resonances. The data are fitted with these two background contributions and a Voigt function, with no constraints for energy and angular dependence. In some cases, a residual background is seen for which we have found no explanation. However, the extraction of the K^* signal yields a stable result. This unidentified background may be the reason that in some cases, the ρ density matrix elements scatter more than expected.

The methods 2 to 5 give nearly identical results for all distributions. The results on the differential cross section are fully consistent with those presented in Ref. [4] but differ slightly; we assign these differences due to the systematic uncertainties in the background subtraction and use the difference between the results from Ref. [4] and the fourth method to estimate the systematic uncertainty for the differential cross section; for the ρ density matrix elements we use the mean difference between the first and the fourth method to estimate the systematic uncertainty. The results from Ref. [4] or, respectively, from the fourth method are used as central values. In addition, there is an overall flux uncertainty of $\pm 8\%$. This is included in the error on branching ratios given below.

To extract the density matrices we have fitted every energy and K^{*+} angle bin with the following equation [6]:

$$W(\cos\Theta, \Phi) = \frac{3}{4\pi}\left(\frac{1}{2}(1 - \rho_{00}) + \frac{1}{2}(3\rho_{00} - 1)\cos^2\Theta \right.$$
$$\left. - \sqrt{2}Re\rho_{10}\sin 2\Theta\cos\Phi - \rho_{1-1}\sin^2\Theta\cos 2\Phi\right). \tag{3}$$

Here Θ and Φ are angles of the K_S in the $K^{*+}(892)$ rest system. The events were rotated to have XZ as the reaction plane and
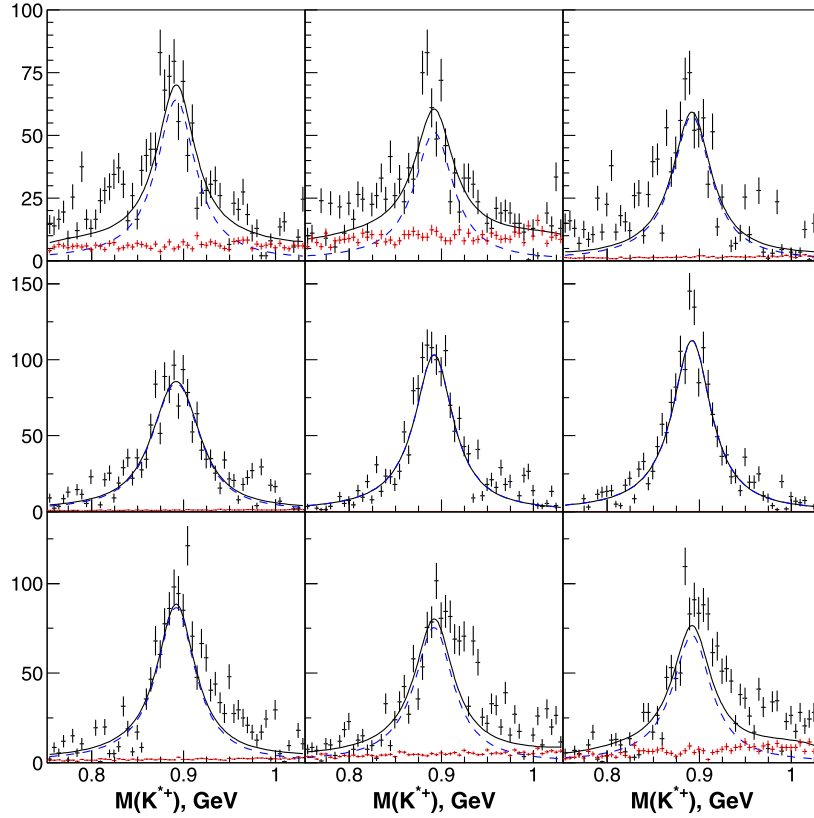
Fig. 3. $K_S^0\pi^+$ invariant mass distributions for $2200 < W < 2300$ MeV and nine equidistant ranges in $\cos\theta$ covering the full angular range, starting from backward angles in the top-left plot. The solid curve represents a fit with a Voigt function (dashed) plus background from a Monte Carlo simulation.

boosted from the center-of-mass system keeping the direction of the Z-axis (Adair system). The function (3) was minimized with an event by event maximum likelihood method with

$$L = \prod_{j}^{N_{data}} \frac{W_j^{data}}{\sum_i^{N_{MC}} W_i^{MC}}, \qquad (4)$$

where W_j is calculated from (3) for each event in the data and Monte Carlo sample. In the likelihood fit, every event was multiplied with its Q factor. Different Q-factor distributions led to slightly modified density matrix elements; these variations are included in the systematic uncertainty. As mentioned above, the systematic errors are determined from the difference between two methods of background substraction. This method was chosen since some distributions (examples are shown in Fig. 3) show a background which is not fully understood. Often, the differences are large enough in these cases. But in some cases, the differences are small leading to (unrealistic) small total errors.

The Λ recoil polarization P is determined from the $\Lambda \to p\pi^-$ decay asymmetry. In this case, the momenta of the proton, the π^- from the Λ decay and the π^+ from $K^{*+} \to K^0\pi^+$ were measured and the K^0 was reconstructed as a missing particle, where the background was subtracted using the two side bands. Full details of the Λ recoil polarization extraction are given in Ref. [7]. The statistical power of the P measurement is limited; it was hence determined for four angular bins only excluding backward production of Λ hyperons. We show the differential cross sections and the ρ density elements in Figs. 4, 5 and the Λ polarization in Fig. 6. Integration of the differential cross section yields the total cross section shown in Fig. 7.

3. Partial wave analysis

The amplitude for photoproduction was fitted in the framework of the P-vector approach [8] where the photon–nucleon interaction is taken into account as production of an initial state. The strong interacting part is treated in the framework of the D-matrix approach where the real part of the loop diagram is calculated using a N/D-based technique. The regularization of the amplitude is achieved by one subtraction. The details of this approach are given in Ref. [9]. The background contributions are obtained from the reggeized exchanges of pseudoscalar, scalar, and vector mesons in the t-channel [9,10].

The primary aim of this study is to search for *missing resonances* and to identify N^* resonances decaying into $K^*\Lambda$. Therefore we limit the fit range for the differential cross section and density matrix elements to $W < 2.6$ GeV even though the fits are shown over the full W range. The new data on $\gamma p \to K^{*+}\Lambda$ are included in the BnGa data base, which contains data on $\gamma p \to \pi N$, ηp, $K^+\Lambda$, $K\Sigma$, $\pi^0\pi^0 p$, $\pi^0\eta p$, $\pi^- p \to K^0\Lambda$, $\pi p \to K\Sigma$, $\pi^- p \to \pi^0\pi^0 p$, and the SAID amplitudes for πN elastic and charge exchange scattering. References to the data base used in the BnGa analysis can be found elsewhere [11–13]. Recent additions can be found on our web page [14]. Those parameters that describe the data fitted earlier were fixed to those from the solution BnGa2014 [13]. A selection of resonances is allowed to decay into $K^*\Lambda$: these couplings as well as parameters for the t-channel exchange amplitudes were fitted freely in all fits discussed here.

First fits with either K^+, K^{*+}, or K_0^{*+} exchanges alone, with no $N^* \to K^*\Lambda$ decays admitted, result in bad descriptions of the data ($\chi^2/N_{data} = 3799/720$ where the error is calculated from the squared sum of statistical and systematic errors in Figs. 4–6); in particular the recoil polarization is predicted to vanish identically.
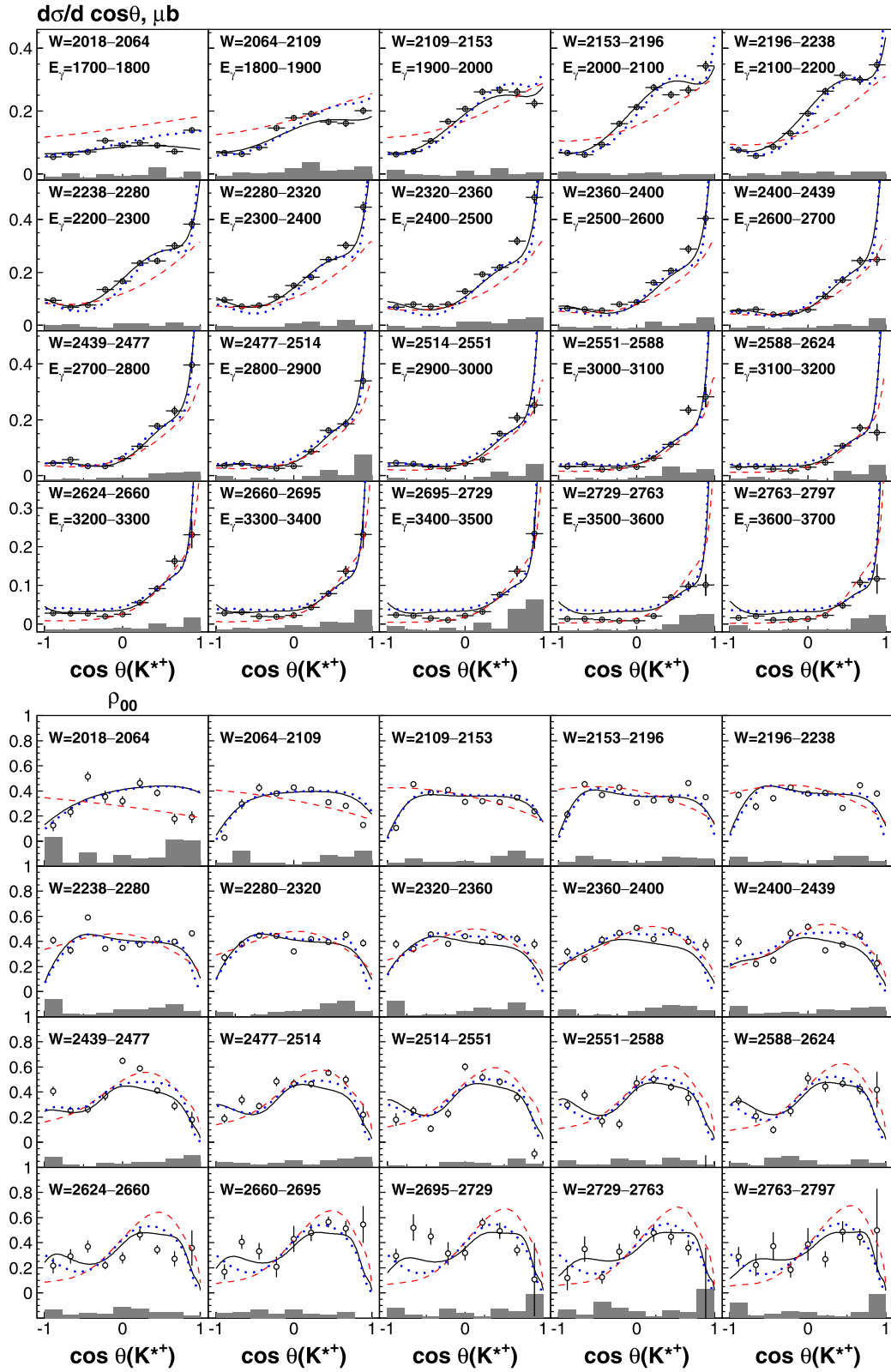
Fig. 4. (Color online.) Differential cross sections (top) and the ρ_{00} and density matrix elements (bottom) for the reaction $\gamma p \to K^{*+}(892)\Lambda$. The uncertainties contain statistical and systematic contributions. The solid curves represent the final BnGa fit, the dashed (red online) curves are fit with t-channel contributions only, the dotted (blue online) curves are fit with the new high-mass resonances omitted. The fits are restricted to invariant mass below 2.6 GeV, making curves at higher energies a prediction.
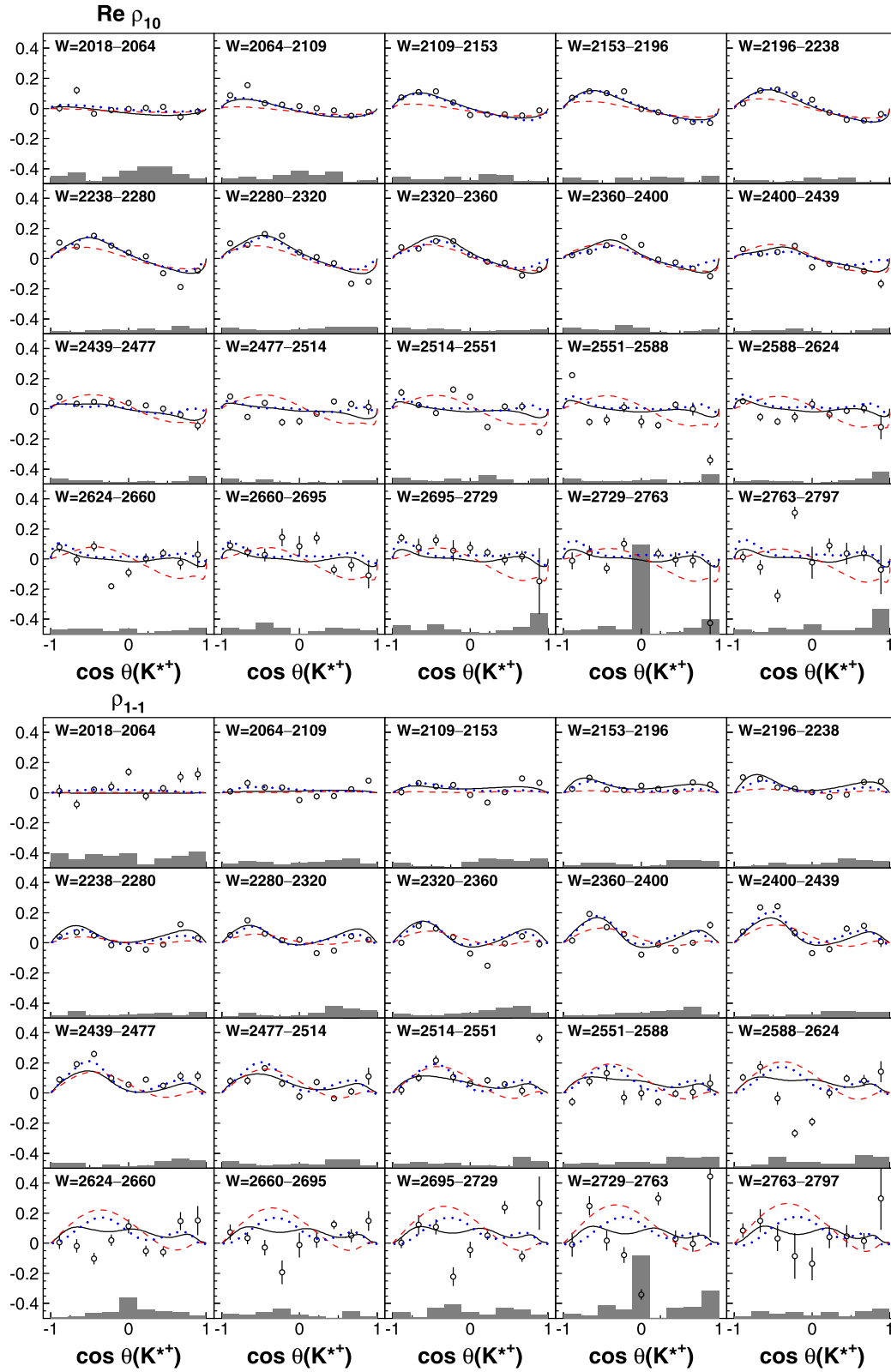
Fig. 5. (Color online.) The ρ_{10} (top) and ρ_{11} (bottom) density matrix elements for the reaction $\gamma p \rightarrow K^{*+}(892)\Lambda$. The uncertainties contain statistical and systematic contributions. The solid curves represent the final BnGa fit, the dashed (red online) curves a fit with t-channel contributions only, the dotted (blue online) curves a fit in which the new high-mass resonances are omitted. The fits are restricted to invariant mass below 2.6 GeV, making curves at higher energies a prediction.
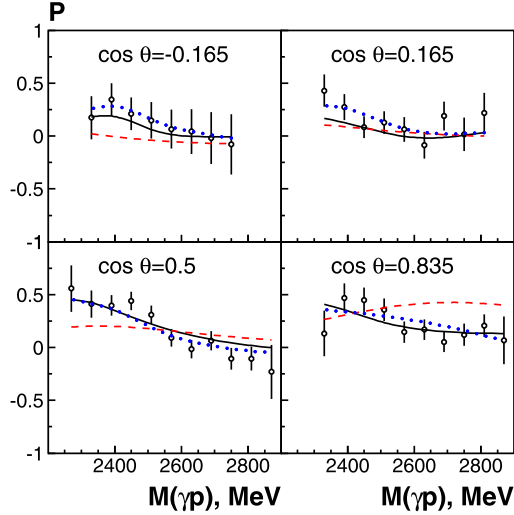
Fig. 6. Recoil polarization of the Λ. The solid curves represent the final BnGa fit, the dashed (red online) curves a fit with t-channel contributions only, the dotted (blue online) curves a fit in which the new high-mass resonances are omitted. The fits are restricted to invariant mass below 2.6 GeV, making curves at higher energies a prediction.

Table 1
Branching ratios for $N^* \rightarrow K^*\Lambda$ decays. For the states denoted with $*$ we assume $\Gamma_{\gamma p} = 0.1$ MeV.

$N(1880)1/2^+$	$0.8 \pm 0.3\%$	$N(1895)1/2^-$	$6.3 \pm 2.5\%$
$N(2100)1/2^+$	$7.0 \pm 4\%$	$N(1875)3/2^-$	$< 0.2\%$
$N(2120)3/2^-$	$< 0.2\%$	$N(2060)5/2^-$	$0.8 \pm 0.5\%$
$N(2000)5/2^+$	$2.2 \pm 1.0\%$	$N(1900)3/2^+$	$< 0.2\%$
$N(2190)7/2^-$	$0.5 \pm 0.3\%$	$N(2355)^*1/2^-$	$6 \pm 1.5\%$
$N(2250)^*3/2^-$	$10 \pm 5\%$	$N(2300)^*5/2^-$	$4.5 \pm 1.4\%$

Table 2
Masses and widths of tentative additional resonances contributing to the reaction $\gamma p \rightarrow K^{*+}\Lambda$.

Resonance	Mass	Width
$N(2355)1/2^-$	2355 ± 20 MeV	235 ± 30 MeV
$N(2250)3/2^-$	2250 ± 35 MeV	240 ± 40 MeV
$N(2300)5/2^-$	2300^{+30}_{-60} MeV	205 ± 65 MeV

With all three t-channel processes admitted, the fit improves considerably, but it is still far from being satisfactory. The χ^2/N_{data} for the differential cross section is 5.64 for the 126 data points, for density matrix elements 4.58 for 378 data points and for recoil polarization 2.59 for 38 data points. The fit exhibits significant deviations between data and fit curve. This fit is shown as dashed (red online) curves in Figs. 4, 5 and 6.

Exploratory fits showed that the subthreshold $N(1895)$ $1/2^-$ and $N(1880)1/2^+$ resonances play an important part in the reaction. We hence tried a fit with t-channel contributions and where the two resonances $N(1895)1/2^-$ and $N(1880)1/2^+$ were allowed to decay into $K^*\Lambda$. The fit improves considerably, χ^2/N_{data} decreases to 3.37 for the differential cross section, to 3.31 for the density matrix elements and to 1.15 for the recoil asymmetry. Restricted to the W region below 2.2 GeV, χ^2/N_{data} goes down to 2.05 for $d\sigma/d\cos\Theta$ (54 points) and to 1.66 for ρ (162 points).

As a next step, we included the $N^* \rightarrow K^{*+}\Lambda$ decays of all resonances used in Ref. [13], i.e., $N(1875)3/2^-$, $N(1880)1/2^+$, $N(1900)3/2^+$, $N(1990)7/2^+$, $N(2000)5/2^+$, $N(2060)5/2^-$, $N(2100)1/2^+$, $N(2190)7/2^-$. Most of the resonances give $N^* \rightarrow K^{*+}\Lambda$ branching ratios with small values, compatible with zero. Those were set to zero in the further fits.

This fit, shown by the dotted (blue online) curves in Figs. 4, 5 and 6, gives a reasonable description of the data with a $\chi^2 = 1.92$ (differential cross section), 1.84 (density matrix elements), and 0.61 recoil asymmetry for 126, 378 and 38 data points, respectively. However, significant deviations are still observed in the mass region 2200–2350 MeV. In particular, the total cross section – obtained by integration of the predicted differential cross section – shows a lack of the intensity in this mass region (and an excess at high energies). Therefore we added to the fit one by one resonances with total spin up to 9/2. Visible improvements of the fits are achieved with added negative-parity resonances with spin $J = 1/2$, 3/2 or 5/2, masses between 2220 and 2350 MeV, and widths in the range of 150 to 300 MeV. Resonances with 7/2 and 9/2 with negative or positive parity provided only marginal improvement and did not fill the lack of intensity in the total cross section.

The best solution is achieved when three states with $J^P = 1/2^-, 3/2^-, 5/2^-$ are introduced to the fit. The fit describes the data with χ^2/N_{data} 0.84, 1.84 and 0.76 (differential cross sec-

tion, density matrix elements, recoil asymmetry). However, the fit is still acceptable when only two of the three resonances are introduced. The three combinations of nucleon resonances with $J^P = 1/2^- + 5/2^-$, $1/2^- + 3/2^-$, and $3/2^- + 5/2^-$ produce the description of very similar quality. The masses and widths of the $J^P = 1/2^-$ and $J^P = 3/2^-$ states are rather stable in all fits, the mass of the $J^P = 5/2^-$ state is somewhat low for the fit with $3/2^- + 5/2^-$ states.

We notice that in highest-energy bins the predicted cross section of the full model (solid curve) is larger than the measured cross section, and that the model with no resonances is closer to the data. However, in the last four mass bins the total χ^2 is 1281 for the full fit (with resonances) and 2120 for the fit without (dashed). The prediction for the ρ density is thus much better for the fit with resonances included. When the last four bins were included in the fit, the masses and widths of the resonances remained stable.

In Table 1 we list the branching ratios for the resonances contributing to the reaction. Here, there is one principle problem: the pole positions of two resonances, $N(1880)1/2^+$ and $N(1895)1/2^-$, are below the threshold for $K^*\Lambda$ decays. Branching ratios are defined at the nominal mass, and hence they vanish when the mass is below the $K^*\Lambda$ threshold or are very small if they are just above. For this reason, we have integrated the $K^*\Lambda$ decay spectrum of these two resonances and normalized this number to the total number of events assigned to the resonance.

The three new resonances have a large product of branching ratios for $N^* \rightarrow N\gamma$ and $N^* \rightarrow K^*\Lambda$. The photocoupling of the new resonances cannot be determined, and hence no definite conclusions can be drawn. In Table 1 it is assumed that the γN partial decay width is about 0.1 MeV.

Here we should add one word of caution. The three resonances listed in Table 2 describe the data but are seen only in this one reaction. It is possible that these resonances actually stand for a large number of resonances expected at these high masses; their common effects might be reasonably well described by a sum of two or three resonances with appropriate spin-parities. Hence the evidence is weak at present that these resonances have the masses, widths, and spin-parities listed in Table 2.

Fig. 7 shows the total cross section for the reaction $\gamma p \rightarrow K^{*+}\Lambda$ and the dominant contributions. At its maximum, the t-channel K and $K_0^*(1430)$ exchange contributions make up more than 50% of the cross section; K^* exchange is also included but is much less pronounced. However all three exchanges together produce a range that is shown by vertical (blue online) hatched region. The sum provides a rather stable fraction of the total cross section (see the enclosed dot-dash region in Fig. 7).
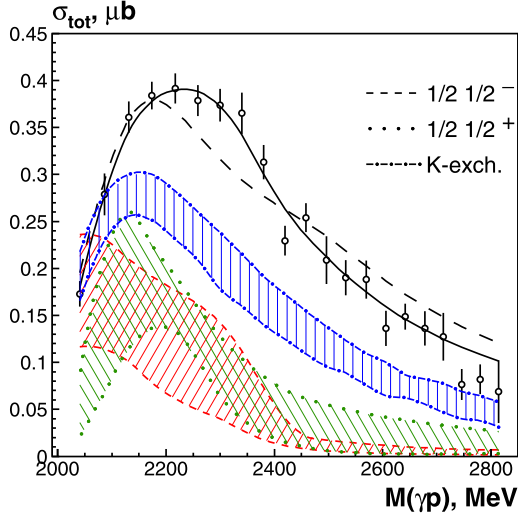
Fig. 7. (Color online.) The total cross section for the reaction $\gamma p \to K^{*+}\Lambda$ and the decomposition into its main components: the sum of t-channel exchanges, and the contributions from the $I = 1/2$, $J^P = 1/2^-$ and $1/2^+$ partial waves. The hatched regions are labeled above, and the solid curve represents the final BnGa fit. The dashed line represents a fit which excludes the three high-mass resonances.

Just above the threshold, the most significant contributions stem from $N(1895)1/2^-$ and the $J^P = 1/2^+$ partial wave with two resonances, $N(1880)1/2^+$ and $N(2100)1/2^+$. The contribution of the $N(1895)1/2^-$ resonance depends on the introduction of the $N(2355)1/2^-$ resonance. The hatched areas shown in Fig. 7 include the range of all fits with two or three high mass states added to the basic solution. The change in the intensity of the $1/2^-$ partial wave influences also the contribution of the $1/2^+$ partial wave to the cross section shown by enclosed dashed region.

4. Discussion and conclusions

Preliminary results on differential cross sections for $\gamma p \to K^{*+}\Lambda$ [15] and $\gamma p \to K^{*0}\Sigma^+$ [16] had been presented at NSTAR 2005. Oh and Kim fitted the differential cross sections and found that K_0^* exchange might provide a significant contribution to the $K^{*0}\Sigma^+$ but is less important for $K^{*+}\Lambda$ [17]. Ozaki, Nagahiro, and Hosaka reproduce the total cross section for $\gamma p \to K^{*+}\Lambda$ [18] assuming that the reaction is dominated by t-channel exchanges. However, their predictions for the energy dependence of the density matrix element show a wrong sign and a wrong energy dependence. Ref. [19] is the first on which addresses possible contributions from N^* resonances. In a fit to the differential cross sections for $2100 < E_\gamma < 2700$ MeV, they find small contributions from two resonances. One is now known as $N(2120)3/2^-$ and a new resonance $N(2200)5/2^-$ (which we might see at 2300 MeV); other partial waves are not investigated, and most intensity is assigned to t-channel exchanges. We notice however that the backward region is not well described. Also the structure seen at $\theta \sim 55°$ is not reproduced by their fit. In a more recent work, S.H. Kim, Hosaka and H.C. Kim reinvestigated $K^*\Lambda$ photoproduction off protons [20]. The comparison of the results of our work with earlier partial wave analyses underlines that t and u-channel contributions are not sufficient to describe the data. The fit in [20] included K^*, K, and K_0^* exchange in the t-channel, Λ, Σ, and Σ^* exchanges in the u-channel, a contact term, and in the s-channel, the nucleon. However, several N^* resonances were required in addition. The latter work presented the most comprehensive analysis; we compare the results from our work with their results.

In [20] the N^* resonances $N(2000)5/2^+$, $N(2060)5/2^-$, $N(2120)3/2^-$, and $N(2190)7/2^-$ were included. The properties of the resonances were fixed to values derived in [11,21] or to values predicted in a relativistic quark model [22]. The $N(2100)1/2^+$ was not included in [20] because of the lack of information. The analysis [20] and the one presented here agree that in the region $E_\gamma < 2.5$ GeV, Born terms contribute about 60% of the total cross section at its peak value (0.4μb) but N^* resonances in the fourth resonance region and above are required to get a good fit. The detailed partial wave contributions remain, however, controversial.

In [20] the N^* resonances $N(2120)3/2^-$ and $N(2190)7/2^-$ provide the strongest contribution; $N(1895)1/2^-$ and $N(2100)1/2^+$ are not tested in [20]. We believe that the data on $\gamma p \to K^{*+}\Lambda$ do require $N(1895)1/2^-$ and contributions from the $J^P = 1/2^+$ wave. $N(1895)1/2^-$ requires an electric dipole transition E_{0+} to be excited, and decays into $K^*\Lambda$ in a relative S-wave. $N(2100)1/2^+$ (and $N(1880)1/2^+$) require magnetic M_{1-} transitions and P-wave decays. These resonances provide the strongest contribution in our analysis. These contributions are missing in [20]; this may be the reason for the poor fit quality for $1.8 \le E_\gamma \le 2.3$ GeV in [20]. Finally, we point out the importance of polarization information for constraining partial wave analyses. Data with beam or target polarization are not available, but here we use at least the recoil polarization and the ρ density matrix elements.

Summarizing, new data on the spin-density matrix elements for the K^* mesons and the Λ recoil polarization produced in the reaction $\gamma p \to K^{*+}\Lambda$ are presented. The data are fitted within the BnGa partial wave analysis. It is found that $N(1895)1/2^-$ and $N(2100)1/2^+$ provide very significant contributions to the reaction. Indications for three new resonances decaying into $K^*\Lambda$ is reported.

References

[1] S. Capstick, W. Roberts, Phys. Rev. D 58 (1998) 074011.
[2] K.A. Olive, et al., Particle Data Group Collaboration, Chin. Phys. C 38 (2014) 090001.
[3] B.A. Mecking, et al., Nucl. Instrum. Methods Phys. Res., Sect. A, Accel. Spectrom. Detect. Assoc. Equip. 503 (2003) 513.
[4] W. Tang, et al., CLAS Collaboration, Phys. Rev. C 87 (2013) 065204.
[5] M. Williams, M. Bellis, C.A. Meyer, J. Instrum. 4 (2009) P10003.
[6] K. Schilling, P. Seyboth, G. Wolf, Nucl. Phys. B 15 (1970) 397.
[7] Wei Tang, PhD dissertation, Ohio University, 2012, http://rave.ohiolink.edu/etdc/view?acc_num=ohiou1351781075.
[8] S.U. Chung, et al., Ann. Phys. 4 (1995) 404.
[9] I. Denisenko, et al., Phys. Lett. B 755 (2016) 97.
[10] A.V. Anisovich, E. Klempt, A. Sarantsev, U. Thoma, Eur. Phys. J. A 24 (2005) 111.
[11] A.V. Anisovich, R. Beck, E. Klempt, V.A. Nikonov, A.V. Sarantsev, U. Thoma, Eur. Phys. J. A 48 (2012) 15.
[12] A.V. Anisovich, E. Klempt, V.A. Nikonov, A.V. Sarantsev, U. Thoma, Eur. Phys. J. A 49 (2013) 158.

[13] V. Sokhoyan, et al., CBELSA/TAPS Collaboration, Eur. Phys. J. A 51 (8) (2015) 95.

[14] http://pwa.hiskp.uni-bonn.de.

[15] I. Hleiqawi, K. Hicks, K^{*0} photoproduction off the proton at CLAS, arXiv:nucl-ex/0512039, in: S. Capstick, V. Crede, P. Eugenio (Eds.), Proc. of the 5th International Workshop on the Physics of Excited Nucleons, NSTAR 2005, 10–15 Oct., 2005, Tallahassee, Florida, World Scientific, Hackensack, USA, 2006.

[16] L. Guo, et al., CLAS Collaboration, Photoproduction of $K^{*+}\Lambda$ and $K^+\Sigma(1385)$ in the reaction $\gamma p \rightarrow K^+\Lambda\pi^0$ at Jefferson lab, in: 5th International Workshop on the Physics of Excited Nucleons NSTAR 2005, 10-15 Oct. 2005, Tallahassee, Florida, World Scientific, Hackensack, USA, 2006, arXiv:hep-ex/0601010.

[17] Y. Oh, H. Kim, Phys. Rev. C 74 (2006) 015208.

[18] S. Ozaki, H. Nagahiro, A. Hosaka, Phys. Rev. C 81 (2010) 035206.

[19] S.H. Kim, S.i. Nam, Y. Oh, H.C. Kim, Phys. Rev. D 84 (2011) 114023.

[20] S.H. Kim, A. Hosaka, H.C. Kim, Phys. Rev. D 90 (1) (2014) 014021.

[21] A.V. Anisovich, V. Burkert, E. Klempt, V.A. Nikonov, A.V. Sarantsev, U. Thoma, Eur. Phys. J. A 49 (2013) 67.

[22] S. Capstick, Phys. Rev. D 46 (1992) 2864.

The CLAS Collaboration

A.V. Anisovich [13,24], K. Hicks [29,*], E. Klempt [13,36], V.A. Nikonov [13,24], A. Sarantsev [13,24], W. Tang [29], D. Adikaram [30], Z. Akbar [11], M.J. Amaryan [30], S. Anefalos Pereira [16], R.A. Badui [10], J. Ball [7], M. Battaglieri [17], V. Batourine [36], I. Bedlinskiy [21], A.S. Biselli [9,5], W.J. Briscoe [12], V.D. Burkert [36], D.S. Carman [36], A. Celentano [17], S. Chandavar [29], T. Chetry [29], G. Ciullo [15], L. Clark [39], P.L. Cole [14], N. Compton [29], M. Contalbrigo [15], V. Crede [11], A. D'Angelo [18,32], N. Dashyan [43], R. De Vita [17], E. De Sanctis [16], A. Deur [36], C. Djalali [34], M. Dugger [2], R. Dupre [20], H. Egiyan [36], A. El Alaoui [37,1,25], L. El Fassi [26], P. Eugenio [11], E. Fanchini [17], G. Fedotov [34,33], A. Filippi [19], J.A. Fleming [38], N. Gevorgyan [43], Y. Ghandilyan [43], K.L. Giovanetti [22], F.X. Girod [36,7], C. Gleason [34], R.W. Gothe [34], K.A. Griffioen [42], L. Guo [10,36], C. Hanretty [41], N. Harrison [36], M. Hattawy [1], M. Holtrop [27], S.M. Hughes [38], Y. Ilieva [34,12], D.G. Ireland [39], B.S. Ishkhanov [33], E.L. Isupov [33], D. Jenkins [40], H. Jiang [34], H.S. Jo [20], S. Joosten [35], D. Keller [41], G. Khachatryan [43], M. Khandaker [14,28], W. Kim [23], F.J. Klein [6], V. Kubarovsky [36,31], L. Lanza [18], P. Lenisa [15], K. Livingston [39], I.J.D. MacGregor [39], N. Markov [8], B. McKinnon [39], C.A. Meyer [5], M. Mirazita [16], V. Mokeev [36,33], R.A. Montgomery [39], A. Movsisyan [15], E. Munevar [36,12], C. Munoz Camacho [20], G. Murdoch [39], P. Nadel-Turonski [36,6], L.A. Net [34], A. Ni [23], S. Niccolai [20], I. Niculescu [22], M. Osipenko [17], A.I. Ostrovidov [11], M. Paolone [35], R. Paremuzyan [27], K. Park [36,23], E. Pasyuk [36,2], P. Peng [41], W. Phelps [10], S. Pisano [16], O. Pogorelko [21], J.W. Price [3], Y. Prok [30,41], A.J.R. Puckett [8], B.A. Raue [10,36], M. Ripani [17], B.G. Ritchie [2], G. Rosner [39], P. Roy [11], F. Sabatié [7], R.A. Schumacher [5], Y.G. Sharabian [36], Iu. Skorodumina [34,33], G.D. Smith [38], D. Sokhan [38], N. Sparveris [35], I. Stankovic [38], S. Stepanyan [36], S. Strauch [34,12], V. Sytnik [37], Ye. Tian [34], M. Ungaro [36,8,31], H. Voskanyan [43], E. Voutier [20], N.K. Walford [6], D.P. Watts [38], M.H. Wood [4,34], N. Zachariou [38], J. Zhang [36], I. Zonta [32]

[1] *Argonne National Laboratory, Argonne, IL 60439, United States*
[2] *Arizona State University, Tempe, AZ 85287-1504, United States*
[3] *California State University, Dominguez Hills, Carson, CA 90747, United States*
[4] *Canisius College, Buffalo, NY, United States*
[5] *Carnegie Mellon University, Pittsburgh, PA 15213, United States*
[6] *Catholic University of America, Washington, D.C. 20064, United States*
[7] *Irfu/SPhN, CEA, Université Paris-Saclay, 91191 Gif-sur-Yvette, France*
[8] *University of Connecticut, Storrs, CT 06269, United States*
[9] *Fairfield University, Fairfield CT 06824, United States*
[10] *Florida International University, Miami, FL 33199, United States*
[11] *Florida State University, Tallahassee, FL 32306, United States*
[12] *The George Washington University, Washington, DC 20052, United States*
[13] *Helmholtz-Institut für Strahlen-und Kernphysik, Universität Bonn, Germany*
[14] *Idaho State University, Pocatello, ID 83209, United States*
[15] *INFN, Sezione di Ferrara, 44100 Ferrara, Italy*
[16] *INFN, Laboratori Nazionali di Frascati, 00044 Frascati, Italy*
[17] *INFN, Sezione di Genova, 16146 Genova, Italy*
[18] *INFN, Sezione di Roma Tor Vergata, 00133 Rome, Italy*
[19] *INFN, Sezione di Torino, 10125 Torino, Italy*
[20] *Institut de Physique Nucléaire, CNRS/IN2P3 and Université Paris Sud, Orsay, France*
[21] *Institute of Theoretical and Experimental Physics, Moscow, 117259, Russia*
[22] *James Madison University, Harrisonburg, VA 22807, United States*
[23] *Kyungpook National University, Daegu 702-701, Republic of Korea*
[24] *Kurchatov Institute, PNPI, 188300, Gatchina, Russia*
[25] *LPSC, Université Grenoble-Alpes, CNRS/IN2P3, Grenoble, France*
[26] *Mississippi State University, Mississippi State, MS 39762-5167, United States*
[27] *University of New Hampshire, Durham, NH 03824-3568, United States*
[28] *Norfolk State University, Norfolk, VA 23504, United States*
[29] *Ohio University, Athens, OH 45701, United States*
[30] *Old Dominion University, Norfolk, VA 23529, United States*
[31] *Rensselaer Polytechnic Institute, Troy, NY 12180-3590, United States*
[32] *Universita' di Roma Tor Vergata, 00133 Rome Italy*

[33] *Skobeltsyn Institute of Nuclear Physics, Lomonosov Moscow State University, 119234 Moscow, Russia*
[34] *University of South Carolina, Columbia, SC 29208, United States*
[35] *Temple University, Philadelphia, PA 19122, United States*
[36] *Thomas Jefferson National Accelerator Facility, Newport News, VA 23606, United States*
[37] *Universidad Técnica Federico Santa María, Casilla 110-V Valparaíso, Chile*
[38] *Edinburgh University, Edinburgh EH9 3JZ, United Kingdom*
[39] *University of Glasgow, Glasgow G12 8QQ, United Kingdom*
[40] *Virginia Tech., Blacksburg, VA 24061-0435, United States*
[41] *University of Virginia, Charlottesville, VA 22901, United States*
[42] *College of William and Mary, Williamsburg, VA 23187-8795, United States*
[43] *Yerevan Physics Institute, 375036 Yerevan, Armenia*

* Corresponding author.
   E-mail address: hicks@ohio.edu (K. Hicks).